Inorg. Chem. **2005**, *44*, 8277–8284

Theoretical Investigation of Paramagnetic Diazabutadiene Gallium(III)–Pnictogen Complexes: Insights into the Interpretation and Simulation of Electron Paramagnetic Resonance Spectra

Heikki M. Tuononen*,† and Andrea F. Armstrong‡

Department of Chemistry, University of Jyväskylä, P.O. Box 35, FIN-40014 Jyväskylä, Finland, and Department of Chemistry, University of Calgary, Calgary, Alberta, Canada T2N 1N4

Received May 30, 2005

The electronic structures and the spin density distributions of the paramagnetic gallium 1,4-diaza(1,3)butadiene (DAB) model systems {(^{t}Bu-DAB)Ga(I)[Pn(SiH_3)$_2$]}$^\bullet$ and the related dipnictogen species {(^{t}Bu-DAB)Ga[Pn(SiH_3)$_2$]$_2$}$^\bullet$ (Pn = N, P, As) were studied using density functional theory. The calculations demonstrate that all systems share a qualitatively similar electronic structure and are primarily ligand-centered π-radicals. The calculated electron paramagnetic resonance (EPR) hyperfine coupling constants (HFCCs) for these model systems were optimized using iterative methods and were used to create accurate spectral simulations of the parent radicals {(^{t}Bu-DAB)Ga(I)[Pn($SiMe_3$)$_2$]}$^\bullet$ (Pn = N, P, or As) and {(^{t}Bu-DAB)Ga[Pn($SiMe_3$)$_2$]$_2$}$^\bullet$ (Pn = P or As), the EPR spectra of which had not been simulated previously due to their complexity. Excellent agreement was observed between the calculated HFCCs and the optimum values, which can be considered the actual HFCCs for these systems. The computational results also revealed inconsistencies in the published EPR data of some related paramagnetic group 13–DAB complexes.

Introduction

Research into the chemistry of inorganic radicals of main group elements has undergone a renaissance in recent years.[1] Since many of the p-block elements have at least one naturally occurring spin-active isotope, the electron paramagnetic resonance (EPR) spectra of these radicals are often quite complex due to hyperfine interactions of the unpaired electron with several magnetically active nuclei. The resultant poor resolution of these EPR spectra renders it difficult to extract accurate values of the hyperfine coupling constants (HFCCs) to the various spin-active nuclei. Because HFCCs are used to glean information regarding the spin density and spin distribution of the unpaired electron throughout a paramagnetic molecule,[2] this is quite problematic, as it can impede researchers from gaining a thorough understanding of a particular radical system. One approach to overcoming this difficulty is to use density functional theory (DFT) calculations to predict the magnitudes of the HFCCs. The calculated values can then be incorporated into a simulation of the experimental EPR spectrum, which, once optimized, yields accurate HFCCs. We have recently shown this methodology to be successful in assigning and interpreting the complex EPR spectra of both tetraimidophosphate[3] and boramidinate[4] radicals.

The 1,4-diaza(1,3)butadiene ligand (DAB) (**1**) readily undergoes a one-electron reduction to form the monoanionic diazabutadiene radical (**2**). By incorporating bulky substituents such as *tert*-butyl- or 2,6-diisopropylphenyl on the nitrogen atoms and chelating this bidentate anion radical to a metal center, it has been proven possible to produce a series of stable paramagnetic compounds. Complexes of aluminum[5] and gallium[6−8] have been reported where the metal is bischelated by one DAB anion radical, **2**, and a neutral DAB

* To whom correspondence should be addressed. Telephone: +358-14-260-2618. Fax: +358-14-260-2501. E-mail: hetuonon@cc.jyu.fi.
† University of Jyväskylä.
‡ University of Calgary.

(1) For a recent review, see: Power, P. P. *Chem. Rev.* **2003**, *103*, 789.
(2) See, for example: Weil, J. A.; Bolton, J. R.; Wertz, J. E. *Electron Paramagnetic Resonance: Elementary Theory and Practical Applications*; Wiley-Interscience: New York, 1994.
(3) (a) Armstrong, A. F.; Chivers, T.; Tuononen, H. M.; Parvez, M. *Inorg. Chem.* **2005**, *44*, 5778. (b) Armstrong, A. F.; Chivers, T.; Tuononen, H. M.; Parvez, M.; Boeré, R. T. *Inorg. Chem.*, in press.
(4) Chivers, T.; Eisler, D. J.; Fedorchuk, C.; Schatte, G.; Tuononen, H. M.; Boeré, R. T. *Chem. Commun.* **2005**, 3930.
(5) Cloke, F. G. N.; Dalby, C. I.; Henderson, M. J.; Hitchcock, P. B.; Kennard, C. H. L.; Lamb, R. N.; Raston, C. L. *J. Chem. Soc., Chem. Commun.* **1990**, 1394.

10.1021/ic050864r CCC: $30.25
Published on Web 10/19/2005

ligand, **1**, forming a spirocyclic ligand-centered monoradical; isostructural radicals of the s-block metals lithium and magnesium are also known.[9]

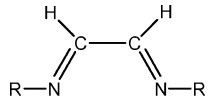

1

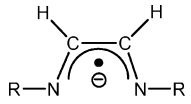

2

More recent developments in this area have resulted in the isolation and characterization of a wide range of paramagnetic DAB complexes of the group 13 metals, particularly gallium.[7,8,10−12] Among these are the monocyclic pnictogen compounds {(^{t}Bu-DAB)Ga(I)[Pn(SiMe$_3$)$_2$]}$^\bullet$ (**3a**, Pn = N; **4a**, Pn = P; **5a**, Pn = As) and the related dipnictogen species {(^{t}Bu-DAB)Ga[Pn(SiMe$_3$)$_2$]$_2$}$^\bullet$ (**7a**, Pn = P; **8a**, Pn = As), though the nitrogen analogue of the latter radicals {(^{t}Bu-DAB)Ga[N(SiMe$_3$)$_2$]$_2$}$^\bullet$ (**6a**) has not been isolated.[13] The EPR spectra of these novel radicals are quite complex due to hyperfine couplings to the ^{1}H and ^{14}N nuclei of the DAB backbone, as well as to ^{69,71}Ga (^{69}Ga, 60%, I = $^3/_2$; ^{71}Ga, 40%, I = $^3/_2$), the pnictogen atom(s) (^{14}N, 99%, I = 1; ^{31}P, 100%, I = $^1/_2$; ^{75}As, 100%, I = $^3/_2$), and the iodine nucleus (^{127}I, 100%, I = $^5/_2$) in the case of **3**−**5**.

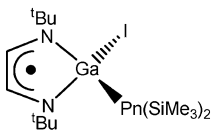

3–5

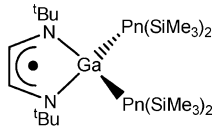

6–8

At present, accurate simulations of the EPR spectra of **3a**−**5a**, **7a**, and **8a** have not been obtained due to their complexity: though the magnitudes of some of the HFCCs have been estimated, these values alone do not accurately reproduce the experimental spectra. Additional complications in simulating these spectra have been attributed to "slight differences in ^{69,71}Ga hyperfine couplings and isotropic *g*-values".[13] However, the electronic Zeeman interaction does not depend on nuclear isotopes.[2] In addition, the HFCCs of ^{69}Ga and ^{71}Ga isotopes in a given magnetic environment are inter-related by the ratio of their nuclear *g*-factors provided that the EPR spectrum shows no significant anisotropy.[2] The near-perfect inversion symmetry with respect to peak positions exhibited by the experimental EPR spectra of these radicals indicates the presence of negligible amounts of anisotropy.

A recent theoretical investigation[14] of a series of paramagnetic group 13−DAB complexes has indicated that the singly occupied molecular orbitals (SOMOs) of these systems are compositionally equivalent and, like their spin density distributions, exhibit only a minor dependence upon the identity of the central metal and the substituents which complete its coordination sphere. The magnitudes of the HFCCs for these ligand-centered π-radicals were calculated and found to be in very good agreement with values extracted from experimental EPR spectra, in cases where the identity of the paramagnetic species has been definitively established. In light of these results, we have now undertaken a DFT study of the pnictogen-containing radicals **3**−**8** in order to determine their electronic structures and spin density distributions. The complex EPR spectra of these radicals will then be interpreted in terms of their electronic structures and predicted HFCCs. Some implications of these results regarding the characterization of other know group 13−DAB complexes are also discussed.

Computational Details

The geometries of the radical systems {(^{t}Bu-DAB)Ga(I)[Pn(SiH$_3$)$_2$]}$^\bullet$ (**3b**, Pn = N; **4b**, Pn = P; **5b**, Pn = As) and {(^{t}Bu-DAB)Ga[Pn(SiH$_3$)$_2$]$_2$}$^\bullet$ (**6b**, Pn = N; **7b**, Pn = P; **8b**, Pn = As) were optimized in their doublet ground states using DFT. The calculations utilized the hybrid PBE0 exchange-correlation functional[15] and Ahlrichs' triple-ζ valence basis sets augmented by one set of polarization functions (TZVP).[16] For iodine, the corresponding large-core ECP basis sets (46 electrons frozen) were used.[16] The PBE0 hybrid density functional was chosen on the grounds of several published benchmarks that have shown it to perform well in calculating molecular properties for a wide variety of chemical systems.[17] The way in which the PBE0 functional is constructed and the lack of empirical parameters fitted to specific physical properties also render it appealing from a purely theoretical standpoint. Appropriate molecular point groups were used to improve the efficiency of the calculations.

Hyperfine coupling constants were calculated for **3b**−**5b** in their geometry optimized structures using both quasi-relativistic and fully relativistic methods and the unrestricted Kohn−Sham formalism. For compounds **6b**−**8b**, only nonrelativistic calculations were done. The nonrelativistic calculations utilized the same TZVP basis sets and density functional as the geometry optimizations; several benchmarks have recently been published which demonstrate the suitability of the TZVP basis set for the calculation of EPR

(6) Cloke, F. G. N.; Hanson, G. R.; Henderson, M. J.; Hitchcock, P. B.; Kennard, C. H. L.; Raston, C. L. *J. Chem. Soc., Chem. Commun.* **1989**, 1002.

(7) Pott, T.; Jutzi, P.; Neumann, B.; Stammler, H.-G. *Organometallics* **2001**, *20*, 1965.

(8) Baker, R. J.; Farley, R. D.; Jones, C.; Mills, D. P.; Kloth, M.; Murphy, D. M. *Chem.—Eur. J.* **2005**, *11*, 2972.

(9) Gardiner, M. G.; Hanson, G. R.; Henderson, M. J.; Lee, F. C.; Raston, C. L. *Inorg. Chem.* **1994**, *33*, 2456.

(10) Pott, T.; Jutzi, P.; Kaim, W.; Schoeller, W. W.; Neumann, B.; Stammler, A.; Stammler, H.-G.; Wanner, M. *Organometallics* **2002**, *21*, 3169.

(11) Baker, R. J.; Farley, R. D.; Jones, C.; Kloth, M.; Murphy, D. M. *Chem. Commun.* **2002**, 1196.

(12) Baker, R. J.; Farley, R. D.; Jones, C.; Kloth, M.; Murphy, D. M. *Dalton Trans.* **2002**, 3844.

(13) Antcliff, K. L.; Baker, R. J.; Jones, C.; Murphy, D. M.; Rose, R. P. *Inorg. Chem.* **2005**, *44*, 2098.

(14) Tuononen, H. M.; Armstrong, A. F. *Dalton Trans.*, submitted for publication.

(15) (a) Perdew, J. P.; Burke, K.; Ernzerhof, M. *Phys. Rev. Lett.* **1996**, *77*, 3865. (b) Perdew, J. P.; Burke, K.; Ernzerhof, M. *Phys. Rev. Lett.* **1997**, *78*, 1396. (c) Perdew, J. P.; Burke, K.; Ernzerhof, M. *J. Chem. Phys.* **1996**, *105*, 9982. (d) Ernzerhof, M.; Scuseria, G. E. *J. Chem. Phys.* **1999**, *110*, 5029.

(16) The basis sets were used as they are referenced in the Turbomole 5.7.1 internal basis set library. These basis sets can be downloaded from ftp://ftp.chemie.uni-karlsruhe.de/pub/basen/for free of charge. This site was accessed in May 2005.

(17) (a) Adamo, C.; Barone, V. *J. Chem. Phys.* **1999**, *110*, 6158. (b) Adamo, C.; Barone, V. *Chem. Phys. Lett.* **1998**, *298*, 113. (c) Adamo, C.; Barone, V. *THEOCHEM* **1999**, *493*, 145. (d) Adamo, C.; Barone, V. *Theor. Chem. Acc.* **2000**, *105*, 169.

parameters using DFT.[18] For **3b**−**5b**, the use of a quasi-relativistic ECP for the heavier nucleus iodine prevents the direct determination of its HFCCs using the same method. Thus, all-electron relativistic calculations were carried out for the systems with iodine atoms. The calculations utilized the large QZ4P STO basis set, the PBEPBE GGA functional,[15a−c] and the scalar-relativistic ZORA formalism. In quasi-relativistic calculations, large-core ECPs were used on iodine; test calculations showed that virtually the same set of HFCCs was obtained when small-core ECPs were utilized.

All geometry optimizations were done with the Turbomole 5.71[19] and Gaussian 03[20] program packages. The hyperfine coupling constant calculations were done with the Gaussian 03[20] (nonrelativistic and quasi-relativistic) and ADF 2004.01[21] program packages (fully relativistic). Population analyses were done using the NBO 3.1 program as implemented in Gaussian03.[22] Spectral simulations were carried out using XEMR[23] and WINEPR SimFonia.[24]

Results and Discussion

Gallium−Monopnictogen Diazabutadiene Radicals. Calculations were carried out on the gallium−pnictogen diazabutadiene model systems {(^{t}Bu-DAB)Ga(I)[Pn(SiH_3)$_2$]}$^\bullet$ **3b**−**5b**. As a whole, the calculated bond angles and bond lengths are in good agreement with the values determined by X-ray crystallography for the parent systems {(^{t}Bu-DAB)Ga(I)[Pn($SiMe_3$)$_2$]}$^\bullet$ **3a**−**5a**,[13] taking into account the different electronic and steric effects of the SiH_3 groups compared to the $SiMe_3$ groups. Pertinent calculated and experimental metrical parameters are compiled in Table 1. The geometry-optimized structures of **3b**−**5b** contain a planar DAB ligand chelated to a gallium atom which displays a tetrahedral coordination environment. In the case of **3b**, the Pn(SiH_3)$_2$ nitrogen atom is trigonal planar; for the heavier pnictogen analogues **4b** and **5c**, pyramidal geometries are observed about the group 15 atoms, with the sum of the bond angles totaling 307.1 and 297.9° for phosphorus and arsenic, respectively. This result is consistent with the experimentally determined solid-state structures of **3a**−**5a**.[13] The predicted Ga−Pn (Pn = P, As) bond lengths are consistently slightly longer (0.05 Å) than the experimentally determined distances; conversely, the calculated Ga−I bonds in **4b** and **5b** are shorter (0.03 Å) than the actual bond lengths of **4a** and **5a**. These can be attributed to the different steric and electronic effects of the $SiMe_3$ substituents as compared to the SiH_3 units of the model systems; the discrepancies in Ga−I bond lengths also arise from the quasi-relativistic nature of the calculations. The lesser steric bulk of the SiH_3 groups (cf. $SiMe_3$) is also the reason for the large variance between the calculated and experimental sums of bond angles for the pnictogen atoms (see Table 1). For **3a**/**3b**, where the pnictogen atom (N) is trigonal planar, better agreement between the experimental and calculated structural parameters is observed, as expected.

Despite the difference between the geometries of **3** and **4**/**5**, the SOMOs of **3b**−**5b** were found to be essentially identical, which is in agreement with the π-radical nature of the systems. In all three instances, the SOMO is localized on the DAB ligand and is composed primarily of nitrogen and carbon p-orbitals. The SOMOs have no s-contribution from the central metal or DAB hydrogen atoms and only very small contributions from the pnictogen and iodine nuclei; the SOMO of **5b** is depicted in Figure 1. The Mulliken population analyses of **3b**−**5b** were consistent with the appearance of the SOMOs, indicating that the unpaired

Table 1. Experimental and Calculated Metrical Parameters for **3**−**5**

	3		**4**		**5**	
parameter	calcd[a]	exp[b]	calcd[a]	exp[b]	calcd[a]	exp[b]
r GaN	1.982	1.956	1.981	1.963	1.981	1.957
r GaI	2.587	2.590	2.563	2.589	2.567	2.594
r GaPn	1.881	1.868	2.341	2.291	2.442	2.389
r NC	1.327	1.329	1.328	1.326	1.327	1.318
r CC	1.398	1.406	1.397	1.395	1.397	1.411
∠ NGaN	84.9	85.9	85.0	85.9	85.0	85.6
∠ IGaPn	119.3	118.0	113.6	115.2	113.4	114.9
∠ GaNC	108.6	108.6	108.6	108.2	108.7	108.3
∠ NCC	118.8	118.3	118.7	118.5	118.9	118.5
∑ ∠ Pn	360.0	360.0	307.1	323.3	297.9	316.8

[a] Values calculated for **3b**−**5b**. [b] Averaged experimental values of **3a**−**5a** taken from ref 13.

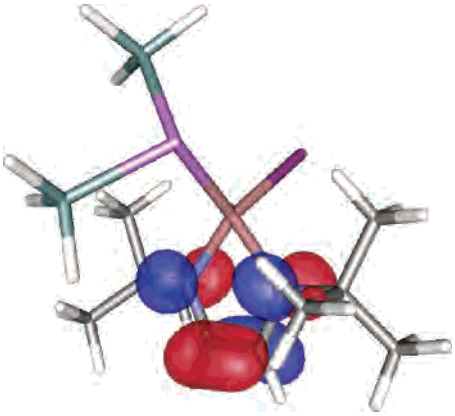

Figure 1. SOMO of {(^{t}Bu-DAB)Ga(I)[As(SiH_3)$_2$]}$^\bullet$, **5b** (isosurface value = ±0.05).

(18) (a) Hermosilla, L.; Calle, P.; Garcia de la Vega, J. M.; Sieiro, C. *J. Phys. Chem. A* **2005**, *109*, 1114. (b) Nguyen, M. T.; Creve, S.; Vanquickenborne, L. G. *J. Phys. Chem. A* **1997**, *101*, 3174. (c) Nguyen, M. T.; Creve, S.; Eriksson, L. A.; Vanquickenborne, L. G. *Mol. Phys.* **1997**, *91*, 537.

(19) Ahlrichs, R.; et al. *TURBOMOLE, Program Package for ab initio Electronic Structure Calculations*, version 5.7.1; University of Karlsruhe: Karlsruhe, Germany, 2004.

(20) Frisch, M. J.; Trucks, G. W.; Schlegel, H. B.; Scuseria, G. E.; Robb, M. A.; Cheeseman, J. R.; Montgomery, J. A.; Vreven, T.; Kudin, K. N.; Burant, J. C.; Millam, J. M.; Iyengar, S. S.; Tomasi, J.; Barone, V.; Mennucci, B.; Cossi, M.; Scalmani, G.; Rega, N.; Petersson, G. A.; Nakatsuji, H.; Hada, M.; Ehara, M.; Toyota, K.; Fukuda, R.; Hasegawa, J.; Ishida, M.; Nakajima, T.; Honda, Y.; Kitao, O.; Nakai, H.; Klene, M.; Li, X.; Knox, J. E.; Hratchian, H. P.; Cross, J. B.; Adamo, C.; Jaramillo, J.; Gomperts, R.; Stratmann, R. E.; Yazyev, O.; Austin, A. J.; Cammi, R.; Pomelli, C.; Ochterski, J. W.; Ayala, P. Y.; Morokuma, K.; Voth, G. A.; Salvador, P.; Dannenberg, J. J.; Zakrzewski, V. G.; Dapprich, S.; Daniels, A. D.; Strain, M. C.; Farkas, O.; Malick, D. K.; Rabuck, A. D.; Raghavachari, K.; Foresman, J. B.; Ortiz, J. V.; Cui, Q.; Baboul, A. G.; Clifford, S.; Cioslowski, J.; Stefanov, B. B.; Liu, G.; Liashenko, A.; Piskorz, P.; Komaromi, I.; Martin, R. L.; Fox, D. J.; Keith, T.; Al-Laham, M. A.; Peng, C. Y.; Nanayakkara, A.; Challacombe, M.; Gill, P. M. W.; Johnson, B.; Chen, W.; Wong, M. W.; Gonzalez, C.; Pople, J. A. *Gaussian 03*, revision C.02; Gaussian, Inc.: Pittsburgh, PA, 2003.

(21) *ADF2004.01*; SCM, Theoretical Chemistry, Vrije Universiteit: Amsterdam, http://www.scm.com.

(22) The population analyses have been done according to the Weinhold−Reed partitioning scheme. For a review, see: Reed, A. F.; Curtiss, L. A.; Weinhold, F. *Chem. Rev.* **1988**, *88*, 899.

(23) Eloranta, J. *XEMR*, version 0.7; University of Jyväskylä: Jyväskylä, Finland, 2004.

(24) *WINEPR SIMFONIA*, version 1.25; Brüker Analytische: Messtechnick, Germany, 1996.

Table 2. NPA Charges (q) and Wiberg Bond Indices (WBI) in Compounds **3b**−**8b**

	DAB		Ga	I	$Pn(SiH_3)_2$		WBI		
compd	q(N)	$q(\Sigma)$	q(Ga)	q(I)	q(Pn)	$q(\Sigma)$	Ga−N	Ga−Pn	Ga−I
3b Pn = N	−0.67	−0.53	1.56	−0.37	−1.83	−0.68	0.33	0.44	0.87
4b Pn = P	−0.65	−0.50	1.21	−0.34	−0.69	−0.37	0.35	0.80	0.89
5b Pn = As	−0.65	−0.50	1.16	−0.35	−0.57	−0.32	0.35	0.83	0.89
6b Pn = N	−0.67	−0.51	1.98		−1.80	−0.73	0.32	0.39	
7b Pn = P	−0.66	−0.50	1.28		−0.70	−0.39	0.34	0.79	
8b Pn = As	−0.66	−0.51	1.18		−0.57	−0.34	0.35	0.82	

electron in each molecule is equally delocalized over the nitrogen and carbon atoms of the DAB backbone (a list of spin densities is included in the Supporting Information).

Since all of complexes **3**−**5** contain a DAB anion radical, **2**, the formal oxidation state on the electropositive gallium centers is +III in all cases. Further analysis using the natural population analysis (NPA) method provides a deeper understanding of the bonding between the gallium and pnictogen/iodine nuclei and facilitates a comparison with the data reported for the related spirocyclic monoradicals $\{Ga(DAB)_2\}^{\bullet}$;[25] the numerical results of these are summarized in Table 2.

As expected, the Ga atom in **3b**−**5b** bears a large positive charge which decreases as the Ga−Pn bond becomes more covalent, i.e., upon descending through the group 15 elements. The DAB anion radical contains a near-constant negative charge of 0.50 electrons; the negative charge is more strongly concentrated on the pnictogen atom on the $Pn(SiH_3)$ group. This is reminiscent of what has been observed for the spirocyclic radicals $\{Ga(DAB)_2\}^{\bullet}$, which display a strong concentration of negative charge on the DAB ring system that has no spin density.[25] The calculated Wiberg bond indices (see Table 2) for **3b** show only a partial bonding character (0.35−0.45) between gallium and the surrounding nitrogen atoms, indicating a strong donor−acceptor character in these bonds. For the heavier pnictogen compounds **4b** and **5b**, the Wiberg index for the Ga−Pn bond approaches unity as the covalent contribution within the bond increases; the Ga−I bond is calculated to be almost purely covalent (Wiberg index of 0.90) for all systems **3b**−**5b**.

The hyperfine coupling constants (HFCCs) for **3b**−**5b** were calculated using both fully relativistic and quasi-relativistic methods and are compiled in Table 3. The HFCCs do not vary significantly from **3b** to **4b** to **5b** except in the following way: the higher symmetry of **3b** due to the trigonal planar geometry of the pnictogen atom renders the ^{1}H and ^{14}N atoms of the DAB ligand symmetry-equivalent. Consequently, the HFCCs to two equivalent ^{1}H and two equivalent ^{14}N atoms are predicted for **3b**, while slight inequivalences are expected for the two ^{1}H and two ^{14}N nuclei of **4b** and **5b**. Relatively small HFCCs have been calculated to the pnictogen atoms of **3b** (0.5 G), **4b** (6.4 G), and **5b** (3.5 G);

Table 3. Experimental and Calculated Hyperfine Coupling Constants (G) for **3**−**5**

	3 (Pn = ^{14}N)		**4** (Pn = ^{31}N)		**5** (Pn = ^{75}As)	
nucleus	calcd[a]	optm[b]	calcd[a]	optm[b]	calcd[a]	exp[c]
^{69}Ga	−19.8 (−15.4)	14.90	−19.6 (−13.5)	10.88	−20.4 (−14.2)	≈36
^{71}Ga	−25.3 (−19.7)	18.80	−25.1 (−17.3)	13.81	−26.1 (−18.2)	≈36
Pn	0.5 (0.5)	1.03	6.4 (7.0)	7.00	3.5 (4.1)	
^{1}H	−5.7 (−5.6)	6.61	−6.0 (−5.7)	6.50	−6.0 (−5.8)	≈1.3
^{1}H	−5.7 (−5.6)	6.61	−5.5 (−5.5)	6.52	−5.4 (−5.4)	≈1.3
^{14}N	4.6 (3.5)	5.48	4.7 (3.5)	5.85	4.7 (3.6)	≈9
^{14}N	4.6 (3.5)	5.48	4.6 (3.6)	5.24	4.6 (3.6)	≈9
^{127}I	0 (16.9)	20.01	0 (17.8)	23.08	0 (18.2)	

[a] Values calculated for **3b**−**5b** using quasi-relativistic and (relativistic) methods. [b] Optimized values used to create the spectral simulation of **3a**−**5a**. [c] Values previously estimated from the experimental spectra (taken from ref 13).

the values of these couplings vary with the relative magnitudes of the gyromagnetic ratios of ^{14}N, ^{31}P, and ^{75}As, as is expected.[2]

The average absolute value of the ^{69}Ga HFCC is 19.9 G using quasi-relativistic methods; this decreases to 14.4 G when a full relativistic ZORA method is applied. Using the quasi-relativistic method, it is not possible to calculate the ^{127}I HFCCs, since an effective core potential is used to model the inner electrons of the iodine atom, which naturally results in near-zero values for these coupling constants. However, fully relativistic calculations have indicated that a significant ^{127}I HFCC should be observed with an average expected magnitude of 17.6 G in **3b**−**5b**; in contrast, the HFCCs to iodine nuclei were assumed to be negligible in the published analysis.[13]

The ^{1}H HFCCs are not expected to change significantly from **3b**−**5b**, nor is there a marked difference between the two inequivalent ^{1}H couplings in either **4b** or **5b**. The range of predicted ^{1}H HFCCs (absolute values vary between 5.4 and 6.0 G) is consistent with those observed in other DAB radicals[9,26] and with those calculated for the related group 13−DAB radicals described elsewhere.[14] Both computational methods yielded similar values of these ^{1}H hyperfine coupling constants, with differences of no more than 0.3 G observed. The ^{14}N HFCCs are similar in magnitude to the ^{1}H couplings but show even less variation throughout systems **3b**−**5b**, with values of either 4.6 or 4.7 G predicted in all instances using quasi-relativistic calculations. These values are in agreement with the ^{14}N HFCCs determined for the DAB nitrogen atoms of a variety of other paramagnetic DAB complexes.[9,26] The implementation of the fully relativistic method appears to result in a significant (1 G) decrease in the ^{14}N HFCCs; however, this is caused by the use of different functionals (hybrid PBE0 vs GGA PBEPBE) and basis sets (TZVP vs QZ4P) for these calculations.[27]

Though precise values of the HFCCs have not been extracted from the experimental EPR spectra of **3a**−**5a**, some conclusions can be drawn regarding the accuracy of the

(25) Schoeller, W. W.; Grigoleit, S. *J. Chem. Soc., Dalton Trans.* **2002**, *405*.

(26) (a) Kaupp, M.; Stoll, H.; Preuss, H.; Kaim, W.; Stahl, T.; van Koten, G.; Wissing, E.; Smeets, W. J. J.; Spek, A. L. *J. Am. Chem. Soc.* **1991**, *113*, 5606. (b) Abakumov, G. A.; Cherkasov, V. K.; Piskunov, A. V.; Druzhkov, N. O. *Dokl. Chem.* **2004**, *399*, 223.

(27) This has been confirmed by carrying out nonrelativistic calculations for **3b**−**5b** using the PBEPBE GGA functional and STO basis sets.

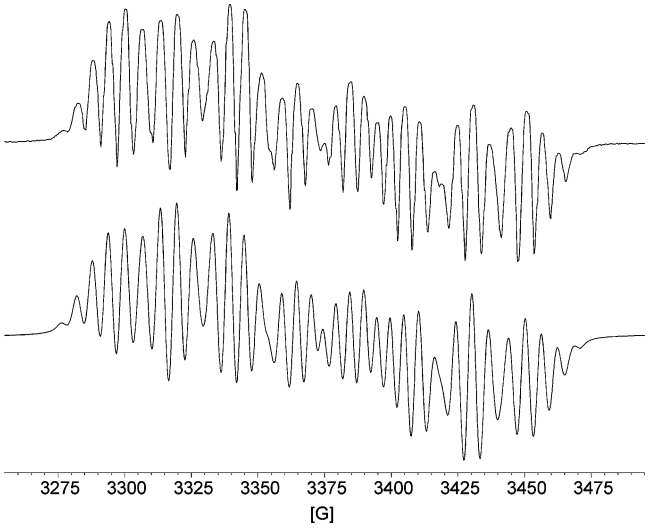

Figure 2. Experimental (top) and simulated (bottom, lw. 2.6 G) EPR spectrum of **3a**. (Experimental spectrum reproduced with permission from ref 13. Copyright 2005 American Chemical Society.)

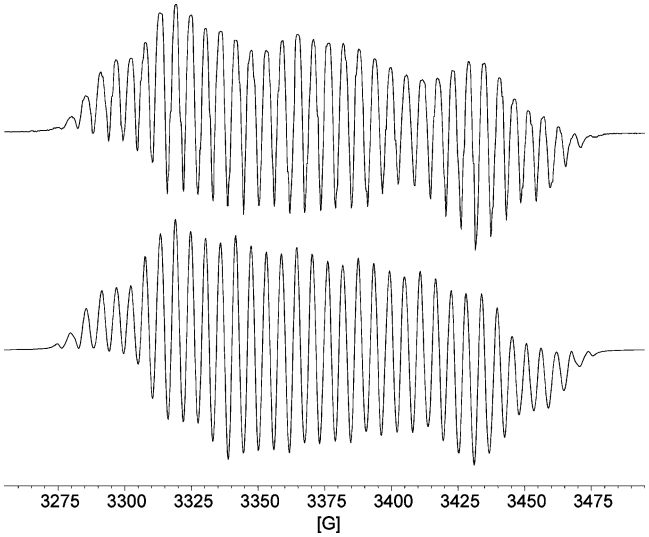

Figure 3. Experimental (top) and simulated (bottom, lw. 2.0 G) EPR spectrum of **4a**. (Experimental spectrum reproduced with permission from ref 13. Copyright 2005 American Chemical Society.)

trends in the calculated HFCCs. First, the calculated HFCCs are quite similar for **3b**−**5b**; consequently, the width of their EPR spectra should be very similar as well. This is borne out in the experimental spectra, where a deviation in width of no more than 10 G is observed from **3a** to **5a**.[13] Second, the experimental spectra are not dominated by the (1:1:1:1) four-line pattern that would be expected if the only large coupling present were to the gallium atom, as had been suggested previously.[13] The appearance of the experimental spectra is thus believed to be influenced equally by the hyperfine couplings to ^{127}I and ^{69,71}Ga, all of which are high-spin nuclei and, thus, have a significant effect on the overall shape of the spectra. In fact, the EPR spectra show a partially concealed sextet pattern due to a large, approximately 20 G, coupling to the spin-$^5/_2$ nucleus ^{127}I.

In light of our recent success in accurately calculating EPR HFCCs for a series of related DAB complexes,[14] attempts were made to simulate the experimental EPR spectra of **3a**−**5a** using the HFCCs that had been calculated for the model systems **3b**−**5b**. Though the calculated values do not accurately reproduce the experimental spectra, optimization of the HFCCs using iterative methods[23] yielded excellent simulations. The experimental and simulated EPR spectra of **3a** and **4a** are shown in Figures 2 and 3, respectively; optimized HFCCs are included in Table 3.[28] The spectral simulation for **3a** was created using identical isotropic *g*-values for both the ^{69}Ga and ^{71}Ga isotopomers and is a near-perfect match with the experimental spectrum. The slight differences between the left- and right-hand sides of the spectrum (i.e., the lack of perfect inversion symmetry in the experimental spectrum with respect to signal intensities) are believed to be caused by higher-order hyperfine interactions due to the presence of large HFCCs to the heavy nuclei ^{69,71}Ga and ^{127}I. To accurately model the experimental spectrum, a third-order perturbation theory based Hamiltonian was utilized when creating the spectral simulation. The HFCCs used to create the simulation are very close to the calculated values for the model system **3b**, with the optimized ^{1}H, ^{14}N, and ^{127}I HFCCs slightly larger than the calculated values, while excellent agreement between the optimized (14.9 G) and calculated (−15.4 G) ^{69}Ga HFCCs is observed.

Similarly, the simulated EPR spectrum of **4a** is in good agreement with the experimental spectrum; this simulation was also created using equivalent isotropic *g*-values for the ^{69,71}Ga isotopomers and a third-order perturbation theory based Hamiltonian. As was seen for **3a**, the optimized ^{1}H, ^{14}N, and ^{127}I HFCCs used to create the spectral simulation of **4a** are slightly larger than the predicted HFCCs to the model system **4b**; conversely, the optimum ^{69}Ga HFCC is 2.6 G smaller than the calculated value. While perfect agreement between the optimized and calculated ^{31}P HFCCs is observed, it must be noted that the assignment of this HFCC to the pnictogen atom phosphorus rather than to one of the DAB hydrogen atoms is somewhat arbitrary, since both ^{1}H and ^{31}P are spin-$^1/_2$ nuclei with a relative natural abundance of 100%. However, a ^{1}H HFCC of 7 G seems somewhat improbable when this value is compared to the ^{1}H couplings present in other related paramagnetic group 13−DAB complexes,[9,26] lending support to the assignment of this coupling to the phosphorus atom. Though intuitively the EPR spectrum of **3a** would be expected to consist of more lines than that of **4a** due to the presence of the higher spin group 15 element nitrogen (^{14}N, $I = 1$; cf. ^{31}P, $I = {}^1/_2$), the ^{14}N HFCC is so small (1.03 G) compared to the experimental line width (2 G) that it remains unresolved and does not produce additional spectral lines. Consequently, the EPR spectrum of **3a** actually contains fewer lines (32) than that of **4a** (36). It is also noted that the optimized HFCCs for both **3a** and **4a** include couplings which are approximately multiples of each other (see Table 3): this accidental degeneracy of lines makes the spectra deceptively

(28) It should be noted that very minor distortions of the line-shape of the experimental EPR spectra occurred through digitization of the spectra for compatibility with the selected EPR software. For high quality versions of the experimental spectra, see ref 13.

simple and complicates extraction of accurate HFCCs solely by means of spectral simulations.[29]

The experimental EPR spectrum of the arsenic analogue **5a** is not as well resolved as those of **3a** and **4a** due to the hyperfine coupling of the unpaired electron with the spin-$^3/_2$ nucleus ^{75}As. Because of the resultant line-broadening, it is more difficult to ascertain whether a given spectral simulation is a definitive match. However, a reasonable simulation of this spectrum (not shown) can be obtained by including HFCCs similar to those used to create the simulation of **4a**, substituting an ^{75}As HFCC of 3.0 G in place of the ^{31}P HFCC of **4a**.

Compounds **3a**−**5a** have also been characterized by ENDOR spectroscopy,[13] which has indicated the presence of ^{1}H HFCCs of approximately 1.4 G in all cases: no larger ^{1}H couplings were detected. No explanation for this observation can be made at this time, as both the calculated HFCCs and spectral simulations support the presence of much larger ^{1}H HFCCs to the hydrogen atoms of the DAB backbone, as does previous work in this area.[9,14,26] In a study of some related DAB-containing radicals,[8] it has proven difficult to detect continuous wave ENDOR signals which result from the DAB-backbone hydrogen atoms due to the broad nature of the resonances: it is possible that a similar effect occurs for **3a**−**5a**. However, the origin of the 1.4 G ^{1}H couplings remains uncertain: they are not thought to arise as a result of the *tert*-butyl substituents of the DAB ligands, as the HFCCs to those methyl protons were calculated to be an order of magnitude smaller. Further research is needed in order to explain the conflicting results.[30]

In the original spectral analyses,[13] the possibility for a significant iodine coupling in **3a**−**5a** was discounted based primarily on results obtained for the related systems {(R-DAB)AlI_2}$^\bullet$ and {(R-DAB)GaI_2}$^\bullet$. For these species, experimental evidence—or rather a lack thereof—has suggested that only minor (<1 G) ^{127}I couplings are present.[8,12] However, an alternative interpretation of the poorly resolved EPR spectrum of {(^{t}Bu-DAB)GaI_2}$^\bullet$ has also been expounded which employs an approximately 8 G HFCC to iodine.[10] In addition, EPR studies on the isoelectronic zinc systems {[(^{t}Bu-DAB)ZnX_2]$^-$}$^\bullet$ (X = Cl, Br), which produce well-resolved spectra, have demonstrated that the bromine derivative displays an approximately 9 G coupling to the heavy halogen ^{79,81}Br.[31] In light of these experimental data, recent computational results,[14] and the present analysis, it appears highly unlikely that the group 13 systems {(R-DAB)MI_2}$^\bullet$ (M = Al, Ga) would exhibit such small HFCCs to iodine as was suggested previously.[8,12]

Gallium−**Dipnictogen Diazabutadiene Radicals.** The model systems {(^{t}Bu-DAB)Ga[Pn(SiH_3)$_2$]$_2$}$^\bullet$ **6b**−**8b** were geometry-optimized and found to be closely structurally related to one another. Each gallium atom displays a tetrahedral coordination sphere; in the case of **6b**, a planar geometry is seen at the pnictogen (N) centers, while both the phosphorus and arsenic atoms of **7b** and **8b**, respectively, are pyramidal. This is reminiscent of the structural trends described above for **3**−**5**. Both {(^{t}Bu-DAB)Ga[Pn($SiMe_3$)$_2$]$_2$}$^\bullet$ (**7a**, Pn = P; **8a**, Pn = As) complexes have been characterized in the solid state by X-ray crystallography and found to be isostructural with each other.[13] The observed pyramidal geometries of the P and As atoms are consistent with the calculated structures of the model systems. Key metrical parameters for the calculated model systems are compiled in Table 4 alongside the corresponding empirical data for **7a** and **8a**. As a whole, the calculated and experimental bond lengths and bond angles are in good agreement with each other; the biggest discrepancies are again observed for the bond angles involving the pnictogen atoms (see Table 4) and arise from the different steric effects of the SiH_3 units in **7b** and **8b** compared to the $SiMe_3$ groups of **7a** and **8a**.

The singly occupied molecular orbitals of **6b**−**8b** were calculated to be essentially identical to those of **3b**−**5b**; the SOMO of **8b** is shown in Figure 4. The Mulliken population analyses indicated that the spin density in **6b**−**8b** is equally distributed over the carbon and nitrogen atoms of the DAB ligand backbone, and only a small contribution from the pnictogen atoms as well as from the gallium nuclei was observed. NAO population analyses displayed similar trends that were also observed for **3b**−**5b** (see Table 2); the Ga−N bonds in **6b** are more ionic in nature, whereas the Ga−P and Ga−As bonds in **7b** and **8b**, respectively, are close to purely covalent.

Table 4. Experimental and Calculated Metrical Parameters for **6**−**8**

	6b	**7**		**8**	
parameter	calcd	calcd[a]	exp[b]	calcd[a]	exp[b]
r GaN	1.989	1.994	1.986	1.996	1.991
r GaPn	1.889	2.363	2.343	2.465	2.437
r NC	1.326	1.328	1.330	1.329	1.328
r CC	1.399	1.396	1.394	1.395	1.382
∠ NGaN	84.5	84.3	84.7	84.3	84.6
∠ PnGaE	117.9	115.8	115.2	115.1	114.7
∠ GaNC	109.0	109.1	108.6	109.0	108.3
∠ NCC	118.7	118.8	119.5	118.9	119.2
∑ ∠ Pn	359.8	305.0	330.4	297.9	322.6

[a] Values calculated for **7b** and **8b**. [b] Averaged experimental values of **7a** and **8a** taken from ref 13.

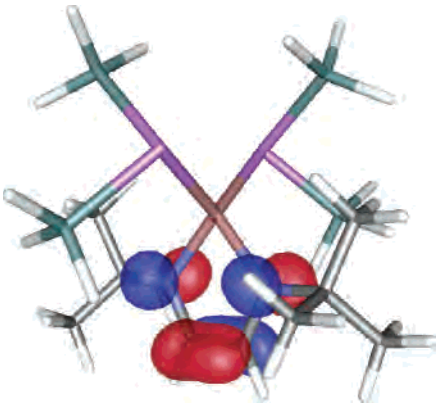

Figure 4. SOMO of {(^{t}Bu-DAB)Ga[As(SiH_3)$_2$]$_2$}$^\bullet$, **8b** (isosurface value = ±0.05).

(29) The same is also true for the HFCCs in radicals **6a**−**8a**.
(30) As originally suggested by our reviewer, it would be highly enlightening to synthesize DAB analogues of **3**−**5** in which the backbone hydrogen atoms have been replaced by deuterium, as this would unambiguously resolve the question of whether there is a large HFCC to the backbone ^{1}H nuclei.
(31) Richter, S.; Daul, C.; von Zelewsky, A. *Inorg. Chem.* **1976**, *15*, 943.

Table 5. Experimental and Calculated Hyperfine Coupling Constants (G) for **6**−**8**

	6 (Pn = ^{14}N)	**7** (Pn = ^{31}P)		**8** (Pn = ^{75}As)	
nucleus	calcd[a]	calcd[a]	optm[b]	calcd[a]	optm[b]
^{69}Ga	−22.0	−22.6	−22.20	−28.2	−25.12
^{71}Ga	−28.2	−28.9	−28.20	−36.1	−31.94
Pn	1.9	9.2	11.70	5.2	8.11
^{1}H	−5.9	−5.6	−4.80	−5.5	5.28
^{14}N	4.4	4.7	5.80	4.8	6.09

[a] Values calculated for model systems **6b**−**8b**. [b] Optimized values used to create spectral simulations of **7a** and **8a**.

Hyperfine coupling constants were calculated for **6b**−**8b**, though the parent nitrogen analogue **6a** has not yet been isolated, and are compiled in Table 5. Since these dipnictogen species do not contain the heavy element iodine, only nonrelativistic calculations were carried out. The higher (C_2) symmetry of **6**−**8** as compared to **4** and **5** renders the hydrogen and nitrogen nuclei on the DAB backbone equivalent by symmetry: consequently, couplings to two equivalent ^{1}H and two equivalent ^{14}N HFCCs are anticipated. The calculated values of the ^{1}H HFCCs for **6b**−**8b** do not differ significantly from the predicted values for **3b**−**5b** or the experimental values obtained for related DAB-centered radicals.[9,26] However, they differ considerably from the values determined in the previously published simulation (*vide supra*).[13] Similarly, little variation is observed between the calculated ^{14}N HFCCs, which range from 4.4 G (**6b**) to 4.8 G (**8b**); these values are again consistent with previous experimental[9,26] and calculated[14] results. The predicted ^{69}Ga coupling constants for **6b**−**8b** are consistently larger than those calculated for the monopnictogen systems **3b**−**5b** due to minor changes in spin density which result from the substitution of a second Pn(SiH$_3$)$_2$ (Pn = N, P, As) unit in place of the iodine atoms of **3b**−**5b**. The only significant difference between the calculated HFCCs for **6b**, **7b**, and **8b** are the values of the pnictogen couplings, which are predicted to be largest for phosphorus (9.2 G) and smallest for ^{14}N (1.9 G), which is consistent with the relative magnitudes of the gyromagnetic ratios of the nuclei.[2] Consequently, any major difference in the appearance of the experimental EPR spectra of **7a** and **8a** is expected to result from the differing HFCCs to the phosphorus (**7a**) and arsenic atoms (**8a**) and from the different nuclear spins of these two isotopes.

Experimental EPR spectra of both **7a** and **8a** have been reported[13] and display near-perfect inversion symmetry, indicating that the higher order hyperfine interactions in these systems are negligible. The EPR spectrum of **8a** is ca. 30 G wider than that of **7a**, which is consistent with the smaller calculated HFCC to the gallium atom of **7a** and the lesser nuclear spin of ^{31}P compared to ^{75}As. An attempt to simulate the experimental EPR spectrum of **7a** using the HFCCs that were calculated for **7b** yielded a spectrum with the correct general features; further optimization of the HFCCs gave an excellent simulation, which is shown in Figure 5. The HFCCs used to create this simulation (Table 5) are very similar to the calculated HFCCs with the most significant deviation observed for the ^{31}P HFCC, which was adjusted by 2.5 G in order to optimize the spectral simulation. Curiously, the calculated ^{1}H HFCC is nearly identical to the optimized ^{14}N HFCC and *vice versa*. Though this suggests that these HFCCs have been assigned incorrectly, the agreement between the simulated and experimental EPR spectra is poor when the optimized ^{1}H and ^{14}N HFCCs are interchanged. The apparently too low and too high values of the calculated ^{14}N and ^{1}H HFCCs, respectively, have been observed in a previous work with related paramagnetic group 13−DAB complexes.[14] This systematic error arises from the apparent tendency of this functional basis set combination[3,4,14] to underestimate couplings which arise due to the spin density of the unpaired electron, such as the DAB−nitrogen atom couplings, while overestimating those which arise due to spin polarization effects, as do the ^{1}H couplings.

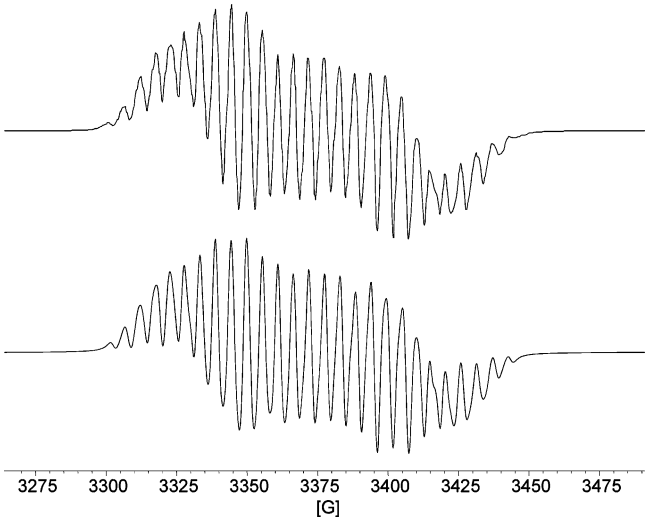

Figure 5. Experimental (top) and simulated (bottom, lw. 2.4 G) EPR spectrum of **7a**. (Experimental spectrum reproduced with permission from ref 13. Copyright 2005 American Chemical Society.)

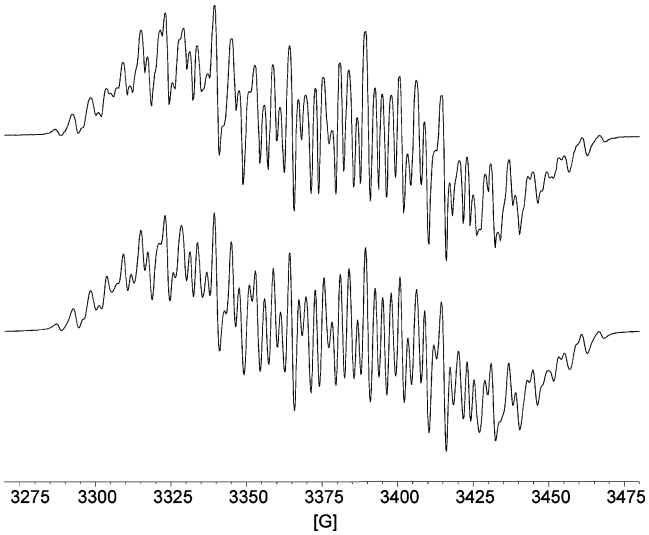

Figure 6. Experimental (top) and simulated (bottom, lw. 1.9 G) EPR spectrum of **8a**. (Experimental spectrum reproduced with permission from ref 13. Copyright 2005 American Chemical Society.)

An excellent simulation (Figure 6) was also obtained for the arsenic-containing radical **8a** by making slight adjustments to the calculated HFCCs of the model system **8b**. As

was seen for **7a**/**7b**, the largest difference between the calculated and optimized couplings occurs for the pnictogen (^{75}As) HFCC; in the case of **8a**/**8b**, the calculated ^{69}Ga HFCC also deviates slightly (2.9 G) from the optimal value. Considering the near-perfect agreement between the simulated and experimental EPR spectra of **7a** and **8a**, the optimized HFCCs derived from these DFT calculations can be regarded as the actual HFCCs present in these systems. Given that both gallium and arsenic are fourth-period elements, the fact that their calculated and actual HFCCs differ by less than 3 G is considered an excellent agreement.

Conclusions

The electronic structures and spin densities of the paramagnetic gallium(III)−pnictogen complexes {(^{t}Bu-DAB)Ga(I)[Pn(SiH_3)$_2$]}$^\bullet$ and {(^{t}Bu-DAB)Ga[Pn(SiH_3)$_2$]$_2$}$^\bullet$ (Pn = N, P, As) were studied using density functional methods. The calculations demonstrate that these π-radicals have qualitatively similar SOMOs with the unpaired electron residing on the DAB backbone. The HFCCs calculated for the model systems were used to simulate the EPR spectra of the closely related radicals {(^{t}Bu-DAB)Ga(I)[Pn($SiMe_3$)$_2$]}$^\bullet$ (Pn = N, P, As) and {(^{t}Bu-DAB)Ga[Pn($SiMe_3$)$_2$]$_2$}$^\bullet$ (Pn = P, As) with excellent accuracy. As shown, the complexity in these EPR spectra does not arise from different isotropic *g*-values for the ^{69}Ga and ^{71}Ga isotopomers, as previously suggested, but from the presence of higher order splitting effects and HFCCs which are approximately multiples of each other. The results also demonstrate the occurrence of significant hyperfine coupling to the ^{127}I nucleus in {(^{t}Bu-DAB)Ga(I)[Pn($SiMe_3$)$_2$]}$^\bullet$ systems as well as confirm the presence of large HFCCs to the ^{1}H atoms in the DAB backbones of both mono- and dipnictogen species. Taken in concert with some previous experimental work, the spectral analyses described herein suggest that the published experimental EPR results of some related paramagnetic group 13−DAB complexes might have been misinterpreted. Detailed theoretical investigations of these systems are currently being pursued in order to resolve this controversy.

Acknowledgment. The authors gratefully acknowledge Helsingin Sanomain 100-vuotissäätiö (H.M.T.) and the University of Calgary (A.F.A.) for financial support.

Supporting Information Available: *XYZ*-coordinates and spin densities of compounds **3b**−**8b.** This material is available free of charge via the Internet at http://pubs.acs.org.

IC050864R